

Article

How Secondary and Tertiary Amide Moieties are Molecular Stations for Dibenzo-24-crown-8 in [2]Rotaxane Molecular Shuttles?

Benjamin Riss-Yaw, Justine Morin, Caroline Clavel and Frédéric Coutrot * 

Supramolecular Machines and ARchitectures Team, Institut des Biomolécules Max Mousseron (IBMM) UMR 5247 CNRS, Université Montpellier, ENSCM, Case Courrier 1706, Bâtiment Chimie (17), 3ème étage, Faculté des Sciences, Place Eugène Bataillon, 34095 Montpellier CEDEX 5, France; benjamin.riss-yaw@etu.umontpellier.fr (B.R.-Y.); justine.morin@etu.umontpellier.fr (J.M.); caroline.clavel@umontpellier.fr (C.C.)

* Correspondence: frederic.coutrot@umontpellier.fr; Tel.: +33-(0)4-6714-3843

Received: 3 November 2017; Accepted: 17 November 2017; Published: 21 November 2017

Abstract: Interlocked molecular machines like [2]rotaxanes are intriguing aesthetic molecules. The control of the localization of the macrocycle, which surrounds a molecular axle, along the thread leads to translational isomers of very different properties. Although many moieties have been used as sites of interactions for crown ethers, the very straightforwardly obtained amide motif has more rarely been envisaged as molecular station. In this article, we report the use of secondary and tertiary amide moieties as efficient secondary molecular station in pH-sensitive molecular shuttles. Depending on the *N*-substitution of the amide station, and on deprotonation or deprotonation-carbamoylation, the actuation of the molecular machinery differs accordingly to very distinct interactions between the axle and the DB24C8.

Keywords: molecular machine; rotaxane; amide; ammonium; amine; dibenzo-24-crown-8; template

1. Introduction

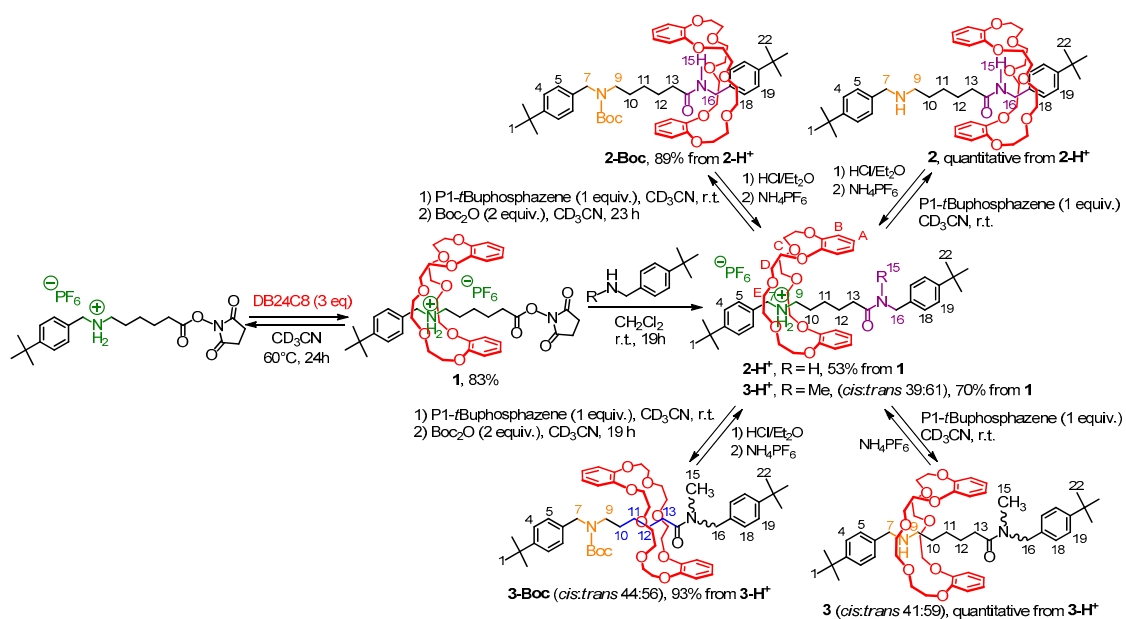
Since the first interlocked molecular shuttles were reported in the literature in 1994 [1,2], several new systems of recognition have been used to control the localization of a macrocycle around either another macrocycle or a thread in more or less sophisticated interlocked molecules. With the dibenzo-24-crown-8 macrocycle (DB24C8), the use of ammonium [3], as template to direct the interlocking process, is probably the most encountered. This template also presents the advantage of being possibly concealed through deprotonation, so that the interactions between the template and the macrocycle become annihilated. This possibility is of interest for the construction of multi-stable molecular shuttles, especially if another thread's moiety of initial weaker affinity is present in the thread. In this case, the macrocycle can shuttle along the thread and sit around the second station. The process can be reversible through protonation. Hence, reporting new stations of weaker affinity for the macrocycle might be of interest. Several secondary stations for the DB24C8 have been reported in the literature to date. As a non-comprehensive list of them, we can cite the following positively charged stations: bipyridinium [4–10], 1,2-bis-(pyridinium)ethane [11–21], triazolium [22–30], pyridinium [31–33], pyridinium amide [34–37], imidazolium [38–41] moieties, oxidized ferrocene [42], etc. Some neutral molecular stations are also important to be mentioned, such as urea [43], thiourea [44], carbamate [45–50], isoxazole [51], and benzylic ester [52], that usually interact either through π - π stacking with the aromatic rings of the crown ether, or through hydrogen bonding with the oxygen atoms of the crown ether. All of these sites of interactions are weaker stations than the ammonium moiety. However, they are better site of recognitions than the amine moiety that

directly derives from deprotonation of the best ammonium station, allowing the pH-sensitive actuation of the molecular machinery. To the best of our knowledge, although one can find in the literature some DB24C8-containing [2]rotaxanes that involve amide moieties [3,53–55], only a few studies have investigated the utilization of a single secondary amide moiety as an efficient secondary molecular station for the DB24C8 [56,57]. In this paper, we straightforwardly synthesized [2]rotaxane molecular shuttles that combine a strong ammonium station and either a secondary or a tertiary amide station. Depending on the class of the amide station, the molecular machinery actuates differently through the concealing/revealing of the ammonium moiety.

2. Results

2.1. Synthetic Access to Molecular Shuttles

The [2]rotaxane molecular shuttles were obtained from the isolable active ester-containing [2]rotaxane building-block **1** (Scheme 1) [24]. A very efficient slippage process allowed the formation of the *N*-hydroxysuccinimide ester-containing [2]rotaxane **1** in very good yield. Once the rotaxane building-block **1** isolated, addition of either *tert*-butylbenzylamine or *N*-methyl-*tert*-butylbenzylamine provided directly the protonated secondary and tertiary amide-containing [2]rotaxanes **2-H⁺** and **3-H⁺**, respectively.



Scheme 1. Synthesis of secondary and tertiary amide-containing [2]rotaxane molecular shuttles.

At the protonated state, the DB24C8 is localized around the best ammonium station whatever the secondary or tertiary class of the amide. Shuttling of the macrocycle along the thread was then considered upon concealing the ammonium station. Deprotonation and deprotonation-carbamoylation of the ammonium were carried out. The deprotonation appeared quite difficult with standard bases such as tertiary amines, sodium hydroxide or DBU, as we already encountered this problem anteriorly with encircled ammonium moieties in interlocked [2]rotaxane species when no sufficiently strong secondary molecular station was present close to the ammonium one [58]. The use of the strong P1-*t*Bu-tris(dimethyl)phosphazene Schwesinger's base (1 equiv) [59] nevertheless allowed the complete deprotonation of the ammonium moiety in situ. Deprotonation-carbamoylation was also achieved and provided the pure carbamoylated [2]rotaxanes **2-Boc** and **3-Boc** in very good yields (89% and 93%, respectively, after chromatography).

2.2. Characterizations of the Molecular Shuttles

In the secondary amide series, the localization of the DB24C8 at the protonated and deprotonated states ([2]rotaxanes **2-H⁺** and **2**) was demonstrated thanks to ¹H NMR spectroscopy (Figure 1). The comparison between the ¹H NMR spectrum of **2-H⁺** with that of the uncomplexed thread **2u-H⁺** highlights the presence and the localization of the DB24C8 around the best ammonium station (Figure 1a,b). Apart from the obvious appearance of H_{A-E} belonging to the DB24C8, hydrogen atoms H₇ and H₉ that are neighboring the ammonium moiety are both shifted downfield in **2-H⁺** ($\Delta\delta = 0.42$ and 0.25 ppm, respectively) due to their hydrogen bonding interactions with the oxygen atoms of the crown ether. At the same time, hydrogen atoms H₁₀₋₁₃, H₁₅ and in a much lesser extent H₁₆ are more or less shifted upfield in **2-H⁺** ($\Delta\delta = -0.22, -0.29, -0.23, -0.28, -0.36$ and -0.03 ppm, respectively) because they experience the shielding region of the aromatic rings of the DB24C8.

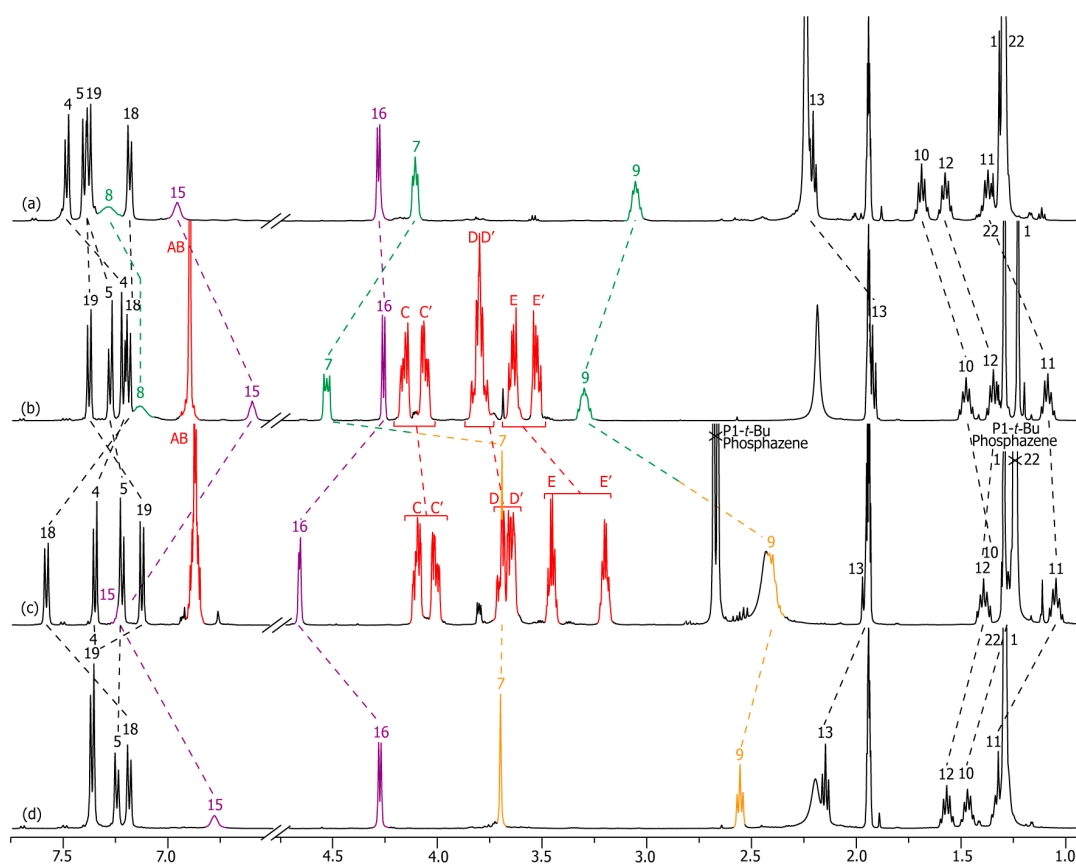


Figure 1. ¹H NMR (500 MHz, CD₃CN, 298 K) comparison between the spectra of: (a) the protonated non-interlocked molecular axle **2u-H⁺**; (b) the protonated [2]rotaxane **2-H⁺**; (c) the deprotonated [2]rotaxane **2**; (d) the deprotonated non-interlocked analogue **2u**. The numbering and coloring of the signals correspond to those indicated in Scheme 1. All the ¹H NMR spectra have been carried out at a concentration of 4.9×10^{-2} M.

Deprotonation of the ammonium triggered the shuttling of the DB24C8 around the secondary amide station (Scheme 1). More precisely, at the deprotonated state of the molecular shuttle, the DB24C8 interacts through hydrogen bonds with the amide hydrogen atom H₁₅ and the next hydrogen atoms H₁₆ (Figure 1b,c). Indeed, with respect to **2-H⁺**, in **2**, the hydrogen atoms H₇, H₉, and in a lesser extent H₁₀ are obviously shifted upfield ($\Delta\delta = -0.91, -0.89,$ and -0.21 ppm, respectively) due to the deprotonation of the ammonium. Meanwhile, hydrogen atoms H₁₅ and H₁₆ are importantly shifted downfield ($\Delta\delta = +0.64$ and $+0.40$ ppm, respectively). Concerning the methylenic hydrogen

atoms $H_{E-E'}$ of the DB24C8, they are shielded in **2** ($\Delta\delta = -0.19$ and -0.32 ppm), because of their localization in the shielding region of the aromatic ring of the *N*-benzylamide extremity of the axle. One might also compare the localization of these hydrogen atoms $H_{E-E'}$ in the two *co*-conformational states **2-H⁺** and **2**. By comparison with the free DB24C8, $H_{E-E'}$ of each *co*-conformational state are shielded in the rotaxane architectures. However, the fact that the DB24C8 interacts with three centers (H_{7-9}) neighboring the aromatic “left” end of the axle at the protonated state **2-H⁺** rather than only two centers (H_{15-16}) next to the aromatic “right” end of the axle in the deprotonated state **2** induces a slight lower shielding of the $H_{E-E'}$ signals in **2-H⁺**.

The accurate localization of the DB24C8 that interacts through hydrogen bonding with only atoms H_{15} and H_{16} in **2** is corroborated by the direct comparison between the 1H NMR spectra of rotaxane **2** and its uncomplexed analogue **2u** (Figure 1c,d). The same trend in chemical shift displacements are observed, i.e., H_{15-16} are the only deshielded hydrogen atoms in the interlocked architecture **2** ($\Delta\delta = +0.46$ and $+0.39$ ppm). It is noteworthy that hydrogen atoms H_{13} , which we imagine they could have interacted through hydrogen bonds with the oxygen atoms of the DB24C8, if one considered the acidity of hydrogen atoms next to an amide carbonyl, are on contrary shielded in the rotaxane **2** ($\Delta\delta = -0.20$ ppm), like H_{9-12} are too ($\Delta\delta = -0.14$, -0.21 , -0.27 , and -0.18 ppm, respectively).

Interestingly, and corroborating the fact that the ammonium moiety was very difficult to deprotonate [36,60], removal of the P1-*t*Bu-tris(dimethyl)phosphazene from the in situ deprotonated rotaxane crude **2** unsuccessfully led, through silica or size-exclusion chromatographic column, to the protonated rotaxane **2-H⁺**. Deprotonation-carbamoylation of rotaxane **2-H⁺** was therefore achieved in order to obtain a pure translational *co*-conformer analogue. Hence, the isolated carbamoylated rotaxane **2-Boc** was easily obtained and isolated in a two-step sequence with an 89% overall yield from **2-H⁺** (Scheme 1). In the [2]rotaxane **2-Boc**, the localization of the DB24C8 along the thread was fully similar to that observed in **2**, highlighting the fact that the presence of the bulky Boc moiety had no influence on the localization of the macrocycle around the secondary amide station. Figure 2 shows the comparison of 1H NMR spectra that are necessary to demonstrate the accurate localization of the macrocycle along the thread. Apart from a difference of chemical shifts for H_7 and H_9 that is due to the carbamoylation of the next amine moiety, exactly the same explanations (downfield shifts due to hydrogen bonds between axle and macrocycle and shielding effect due to aromatic rings of both the DB24C8 and the axle's extremities) can be stated for the system **2-H⁺** / **2-Boc** than those mentioned above for **2-H⁺** / **2**.

Tertiary amide motif was then envisaged in order to evaluate its propensity to act as a secondary molecular station for the DB24C8. To the best of our knowledge, no tertiary amide has been reported as a molecular station for crown ether to date, although one might benefit from the expected weakest affinity of the station for the macrocycle. Since the hydrogen atom, which is linked to the nitrogen atom of a primary or secondary amide, is replaced by a methyl substituent in the tertiary amide-containing rotaxanes **3** and **3-Boc**, we wondered how the DB24C8 would interact with the tertiary amide motif, and if it still does, which hydrogen atoms would be involved in the template site. Remarkably, changing from the secondary to the tertiary class of the amide induced a singular behavior of the macrocycle along the thread, and the localization of the DB24C8 and its interactions with the encircled axle were quite different after deprotonation or deprotonation-carbamoylation of the ammonium template.

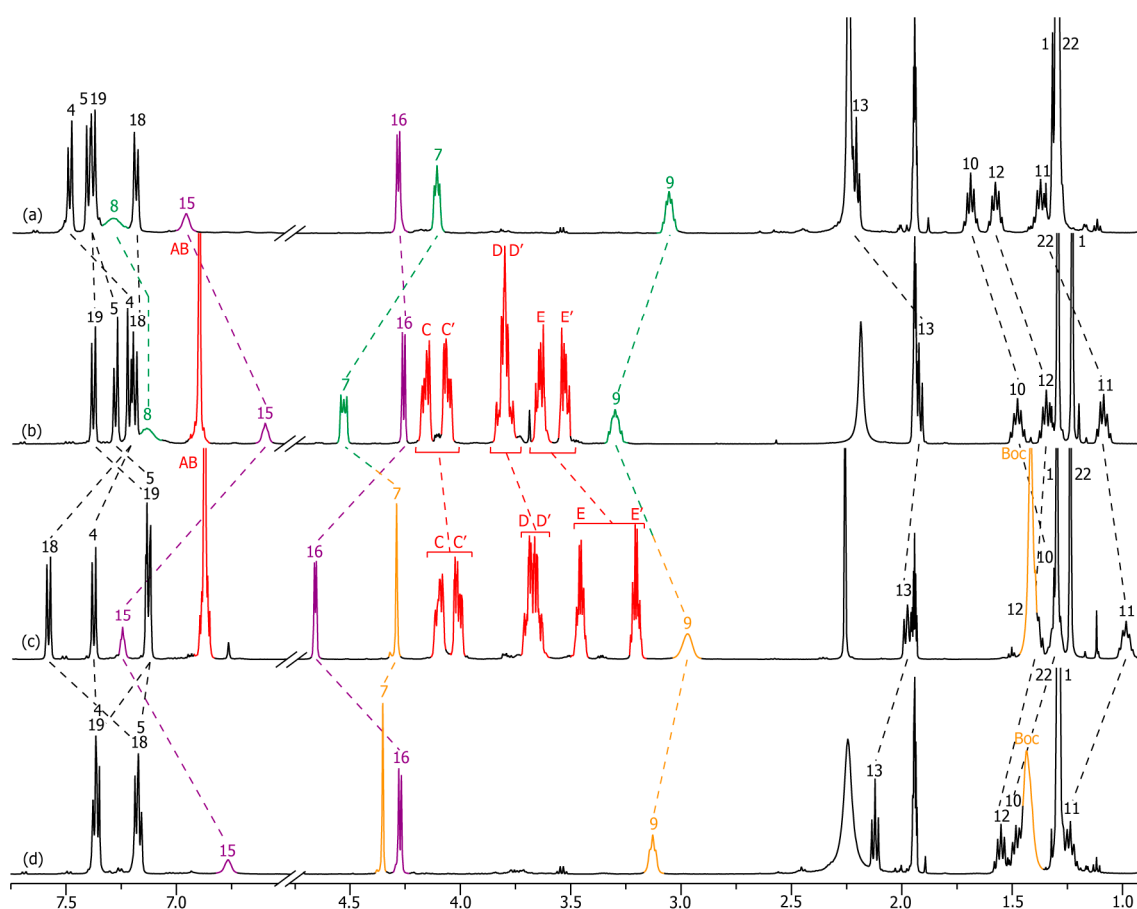


Figure 2. ^1H NMR (500 MHz, CD_3CN , 298 K) comparison between the spectra of: (a) the protonated non-interlocked molecular axle $2\mathbf{u}\text{-H}^+$; (b) the protonated [2]rotaxane 2-H^+ ; (c) the carbamoylated [2]rotaxane 2-Boc ; (d) the carbamoylated non-interlocked analogue $2\mathbf{u}\text{-Boc}$. The numbering and coloring of the signals correspond to those indicated in Scheme 1. All the ^1H NMR spectra have been carried out at a concentration of 4.9×10^{-2} M.

In the protonated rotaxane 3-H^+ , as for 2-H^+ , the DB24C8 resides around the best ammonium station, which appears consistent with the fact that a tertiary amide was expected to be a worse molecular station than the secondary molecular station (Scheme 1, Figure 3). Hence, the same trend of chemical shift variations was noticed when comparing 3-H^+ with its uncomplexed analogue $3\mathbf{u}\text{-H}^+$ than that observed through the comparison between the secondary amide-containing rotaxane 2-H^+ and its uncomplexed analogue $2\mathbf{u}\text{-H}^+$ (Figures 1a,b and 3a,b). Only one difference concerns the higher complexity of the ^1H NMR spectra for the tertiary amide-containing compounds 3-H^+ , 3-Boc , and their respective non-interlocked analogues because of the *cis-trans* isomerism of the amide bond. Briefly, hydrogen atoms H_7 and H_9 are shifted downfield in the interlocked architecture ($\Delta\delta = +0.43$ and $+0.27$ ppm, respectively), due to their implication in hydrogen-bonding with the oxygen atoms of the crown ether, while almost all the other hydrogen atoms are more or less shifted upfield because they experience the shielding effect of the aromatic ring of the DB24C8. Only the hydrogen atoms H_{18-19} and H_{22} do not undergo any variation of their chemical shifts, which corroborates the localization of the DB24C8 at the other side of the encircled axle, i.e., around the ammonium site.

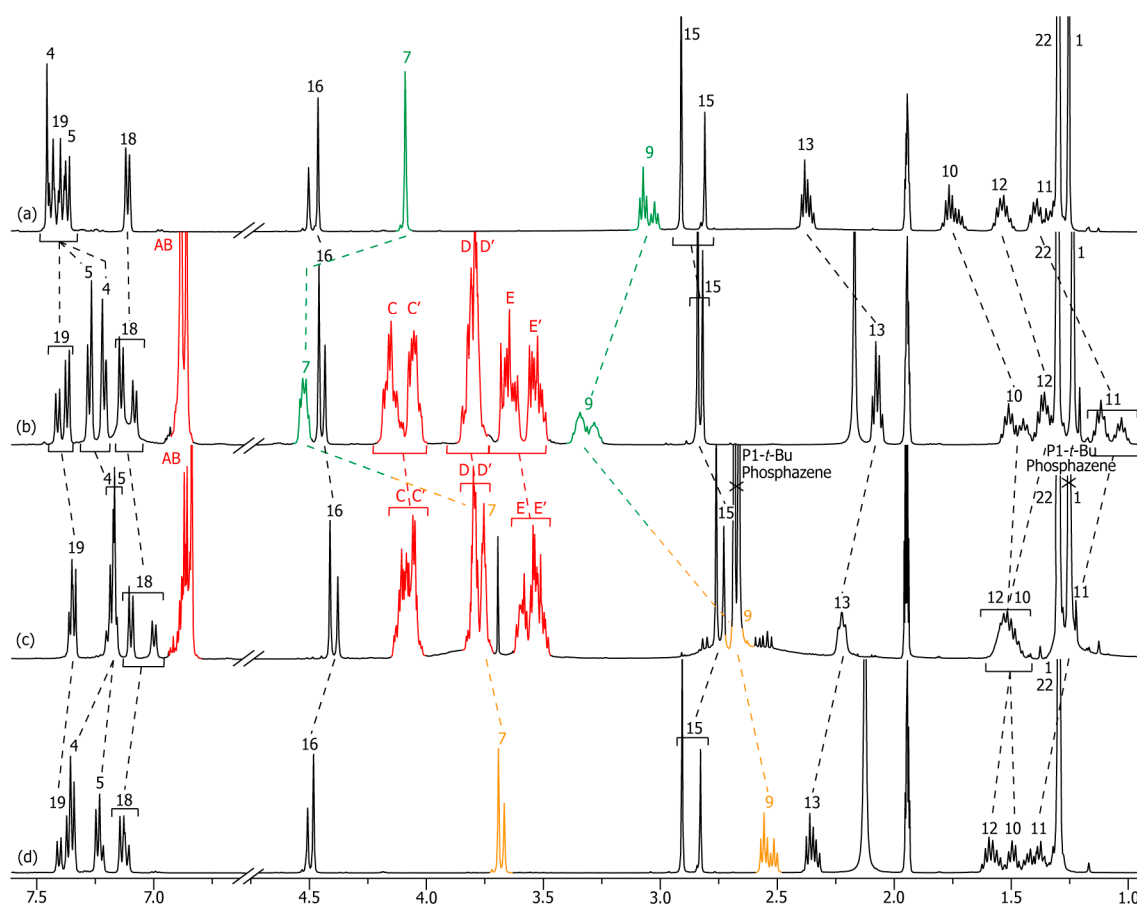


Figure 3. ^1H NMR (500 MHz, CD_3CN , 298 K) comparison between the spectra of: (a) the protonated non-interlocked molecular axle $3\text{u}\text{-H}^+$; (b) the protonated [2]rotaxane 3-H^+ ; (c) the deprotonated [2]rotaxane **3**; (d) the deprotonated non-interlocked analogue **3u**. The numbering and coloring of the signals correspond to those indicated in Scheme 1. All the ^1H NMR spectra have been carried out at a concentration of 4.9×10^{-2} M.

Deprotonation of rotaxane 3-H^+ using the P1-*t*Bu-tris(dimethyl)phosphazene resulted in no real change of the main localization of the macrocycle, albeit an obvious weaker interaction between the interlocked components was noticed. This result implies that the tertiary amide is a weaker molecular station than the amine moiety. The full deprotonation of rotaxane 3-H^+ and the *co*-conformational state of the deprotonated rotaxane **3** are highlighted by the ^1H NMR comparison between spectra of 3-H^+ and **3** (Figure 3b,c). In particular, hydrogen atoms H_7 and H_9 are highly shifted upfield in **3** ($\Delta\delta = -0.77$ and -0.65 ppm, respectively), but not as they should be if they were not interacting with the DB24C8 anymore (see below the comparison between the ^1H NMR spectra of **3** and **3u**). Meanwhile, hydrogen atoms H_{11-13} are deshielded in **3** ($\Delta\delta = +0.19$, $+0.17$, and $+0.15$ ppm, respectively), although the deprotonation of the ammonium moiety provides an amine moiety, which is a lesser electron-withdrawing group. One might therefore suggest that these hydrogen atoms experience a lower shielding effect of the DB24C8 than in 3-H^+ , probably due to the weaker interactions between the amine moiety and the DB24C8 that allow a higher translational degree of freedom of this latter along the thread. This matches with the fact that hydrogen atoms H_{15} and H_{16} (right side of the axle) are slightly shielded in **3** with respect to 3-H^+ ($\Delta\delta = -0.09$ and -0.06 ppm, respectively), which might indicate that they undergo a slight shielding from the aromatic rings of the DB24C8. In fact, the accurate localization of the DB24C8 around the amine in **3** appears slightly different than that observed around the ammonium in rotaxane 3-H^+ . The direct comparison between the ^1H NMR spectra of

3 with that of its uncomplexed analogue **3u** reveals a site of weak hydrogen bonding interactions between the two interlocked components at the amine site (Figure 3c,d). Indeed, one can notice the slight downfield shift of hydrogen atoms H₇ and H₉ in **3** ($\Delta\delta = +0.05$ ppm and $+0.13$ ppm, respectively). Although the macrocycle resides over the same region of the axle in **3** and **3-H⁺** (over the amine or the ammonium region, respectively), the downfield shifts of H₇ and H₉ observed in **3** (with respect to **3u**) are inferior than those observed in the protonated rotaxane **3-H⁺** (with respect to **3u-H⁺**). This is attributed to the weaker hydrogen bonds of the neutral amine station for the DB24C8 with respect to the positively charged ammonium station. More interestingly, the higher downfield shift of H₉ than H₇ ($+0.13$ vs. $+0.05$) in **3** (with respect to **3u**) compared to the higher downfield shift of H₇ than H₉ ($+0.43$ vs. $+0.27$) in **3-H⁺** (with respect to **3u-H⁺**) indicates a small change in the preorganization between the DB24C8 and the axle (the DB24C8 sits more over H₉ than H₇), which corroborates the higher shielding of the “right side” of the axle in **3**. At the exception of H₂₂, all the other hydrogen atoms of the encircled thread are experiencing a slight shielding effect of the aromatic rings of the DB24C8. Besides, the methylenic hydrogens H_{C-E} of the DB24C8 are less split in the deprotonated rotaxane **3** than in **3-H⁺**. This observation corroborates the weaker hydrogen bonds involving the oxygen atoms of the DB24C8 and the amine station since strong hydrogen bonds are known to lower the rotation of σ bonds due to more constrained structure, hence to increase the splitting of the signals due to the better differentiation of geminal hydrogen atoms [36,37].

Surprisingly, deprotonation-carbamoylation of **3-H⁺** resulted in a distinct *co*-conformational state, with respect to what occurred after the single deprotonation of **3-H⁺** (Scheme 1, Figure 4). Indeed, in the [2]rotaxane **3-Boc**, the DB24C8 interacts with the methylenic hydrogen atoms H₁₀₋₁₃ through hydrogen bonding (Figure 4c,d). By comparing the ¹H NMR spectra of the carbamoylated [2]rotaxane **3-Boc** and its uncomplexed thread **3u-Boc**, H₁₀₋₁₃ are shifted downfield in the rotaxane architecture ($\Delta\delta = +0.15$ ppm, $+0.27$ ppm, $+0.21$ ppm, and $+0.18$ ppm, respectively). At the same time, hydrogen atoms H₁₆ (which participate through H-bond with the oxygen atoms of the DB24C8 in the secondary amide-containing [2]rotaxane **2**) are now shielded in **3-Boc** ($\Delta\delta = +0.16$ ppm), probably because the oxygen atoms of the DB24C8 cannot interact with these hydrogen atoms due to the steric problem generated by the amide isomerism. Likewise, hydrogen atoms H₁₅, H₇, H_{Boc} and H₉ are shielded in **3-Boc** ($\Delta\delta = -0.23$, -0.25 , -0.10 , and -0.13 ppm, respectively) because they experience the shielding effect of the aromatic rings of the DB24C8.

It is of particular interest to notice that the expected more acidic hydrogen atoms (i.e., H₁₃) are not the most affected by the hydrogen bonds occurring with the oxygen atoms of the DB24C8. Instead, the next hydrogen atoms H₁₁ and H₁₂ are. One might suggest that both the *cis-trans* isomerism of the next tertiary amide and the rotation of the N-C₁₆ σ bond, which occur quickly at room temperature [61], allow for the presence of isomers in which steric repulsions prevent the DB24C8 from interacting optimally with the most acidic hydrogens H₁₃ (Figure 5b). The DB24C8 is therefore sterically forced to interact with the neighboring less acidic but less hampered hydrogen atoms. More interestingly, the broadening of the ¹H NMR signals in **3**, which are relative to the hydrogen atoms involved in hydrogen bonding interactions with the crown ether, suggests a continuous motion of the macrocycle along the H₁₀₋₁₃ template site of the axle. In this *co*-conformational state, it seems that the DB24C8 tends to interact with the more acidic hydrogen atoms H₁₃, while hindrance due to the rotations of the next amide and N-C₁₆ bonds hampers this interaction. The ROESY ¹H NMR spectrum of **3-Boc** presented in Figure 5a supports this hypothesis, this latter being illustrated in Figure 5b by the cartoon representations of the different conformers. It is particularly important to note the ROE correlation between the aromatic hydrogen atoms H_{18-*cis*} and the most acidic hydrogen atoms H_{13-*cis*}. Highlighted by the cartoon representation of conformer **A** (Figure 5b), this close localization of the stopper with the template site should highly disfavor the expected hydrogen bonding interactions between the oxygen atoms of the DB24C8 and H₁₃ due to steric repulsion. Noteworthy, no correlation exists between the same hydrogen atoms of the *trans* isomer (i.e., H_{13-*trans*} and H_{18-*trans*}), agreeing the cartoon representations of the *trans* isomers **C** and **D**. The existence of conformer **A** is also demonstrated

by the correlation between hydrogen atoms H_{12-cis} and H_{16-cis} , while no correlation are noticed between $H_{12-trans}$ and $H_{16-trans}$ (see Supplementary Materials). The presence of conformers **A-B** are also confirmed by the absence of any correlation between the methylene hydrogen atoms H_{15-cis} and H_{C-E} belonging to the DB24C8 (see Supplementary Materials). This observation supports the fact that the *tert*-butylbenzyl stopper might prevent the DB24C8 from interacting with the close and more acidic hydrogen atoms H_{13} in the *cis* isomers **A** and **B**. It is completely the opposite for $H_{15-trans}$, which strongly correlate with all the hydrogen atoms H_{A-E} of the DB24C8 (see Supplementary Materials). Finally, correlations between H_{10-12} with the methylene hydrogen atoms of the DB24C8 H_{C-E} (see Supplementary Materials) are consistent with the hydrogen-bonding interactions already stated with the help of the 1D 1H NMR spectra comparisons.

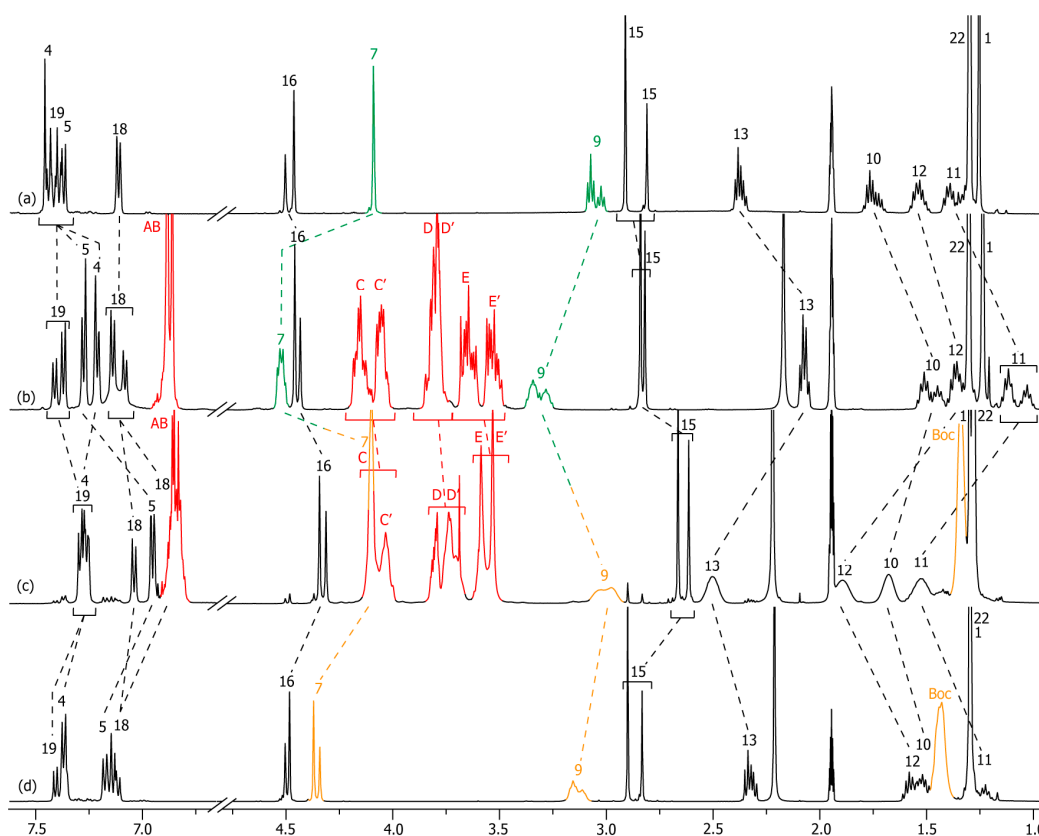


Figure 4. 1H NMR (500 MHz, CD_3CN , 298 K) comparison between the spectra of: (a) the protonated non-interlocked molecular axle $3u-H^+$; (b) the protonated [2]rotaxane $3-H^+$; (c) the carbamoylated [2]rotaxane $3-Boc$; (d) the carbamoylated non-interlocked analogue $3u-Boc$. The numbering and coloring of the signals correspond to those indicated in Scheme 1. All the 1H NMR spectra have been carried out at a concentration of 4.9×10^{-2} M.

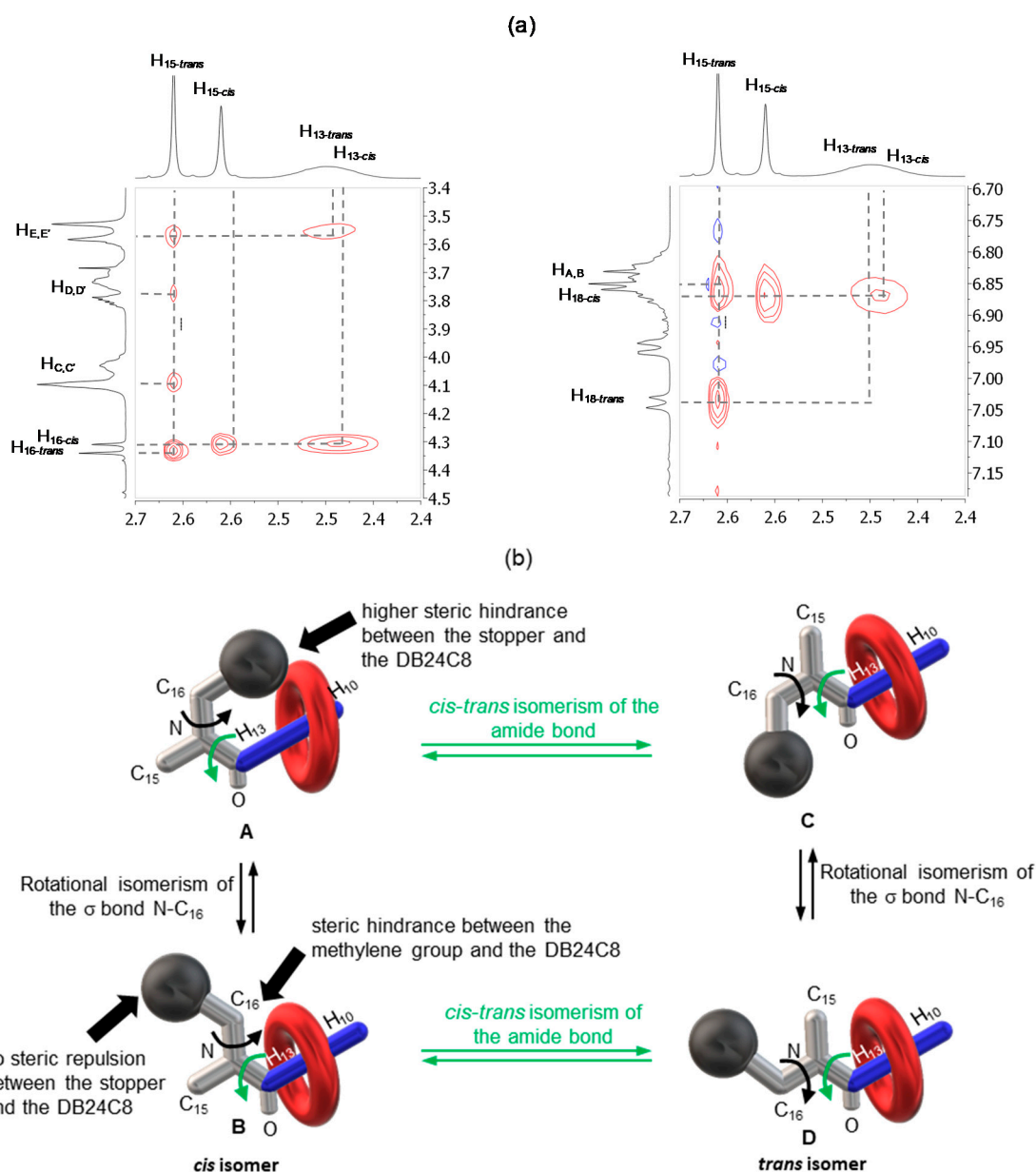


Figure 5. (a) Selected portions of 2D-ROESY ¹H NMR spectrum (500 MHz, CD₃CN, 298 K) of rotaxane 3-Boc; (b) Cartoon representation highlighting the translational motion of the DB24C8 from H₁₀ to H₁₃ due to bonds rotation.

3. Conclusions

In conclusion, we have reported four new DB24C8-based molecular shuttles that contain either a secondary or a tertiary amide station. In the secondary amide series, deprotonation or deprotonation-carbamoylation of the best ammonium station led to a stable *co*-conformational state in which the DB24C8 interacts through hydrogen bonding with both the hydrogen atom linked to the nitrogen of the amide and the benzylic methylene hydrogens. The tertiary amide moiety proved to be a weaker station than the secondary one, although it could act as a secondary station in the case of a deprotonation-carbamoylation of the ammonium. In the case of a sole deprotonation, no shuttling of the DB24C8 around the tertiary amide motif occurred: the DB24C8 stayed around the amine moiety where it interacts through hydrogen bonds, albeit in a different manner than when it resides around the ammonium station. Actually, the DB24C8 prefers to interact with the benzylic methylene hydrogen

atoms neighboring the ammonium rather than with the alkyl methylene group next to the ammonium, while it is the contrary after revealing the amine station. Eventually, deprotonation-carbamoylation resulted in a different behavior of the molecular shuttle in the tertiary amide series. In this case, the concealing of both the ammonium and amine station triggers the shuttling of the DB24C8 towards the amide site, although in a distinct manner than in the secondary amide series. Indeed, the tertiary amide moiety allows for a *cis-trans* isomerism at room temperature that hampers the axle at this site, preventing the DB24C8 from interacting through hydrogen bonds with the hydrogen atoms implied in the secondary amide series. In this case, the DB24C8 sits over the hydrogen atoms borne by the carbons in positions α , β , γ and δ of the carboxamide, where it interacts through hydrogen bonding interactions. More interestingly, due to steric hindrance generated by bonds rotations, the DB24C8 is not localized solely around the expected more acidic hydrogen atoms. It rather seems to adopt a continuous motion over 4 methylene groups. In summary, the DB24C8 can interact through hydrogen bonds with the following stations, albeit with the respective decreasing of affinity: (1) ammonium, (2) *N*-benzylic secondary amide, (3) amine, and (4) *N*-benzylic tertiary amide. New efficient molecular stations of very weak affinity for the macrocycle might be of interest for the conception of multi-stable molecular shuttles with fast shuttling.

Supplementary Materials: Supplementary Materials are available online.

Acknowledgments: B.R.-Y. is funded by the French ministry of research.

Author Contributions: F.C. conceived and designed the experiments. B.R.-Y. and J.M. performed the synthesis and analysis. B.R.-Y., C.C. and F.C. analyzed the data. B.R.-Y., J.M. and C.C. wrote the supplementary materials. F.C. wrote the paper.

Conflicts of Interest: The authors declare no conflict of interest.

References

1. Livoreil, A.; Dietrich-Buchecker, C.O.; Sauvage, J.-P. Electrochemically Triggered Swinging of a [2]-Catenate. *J. Am. Chem. Soc.* **1994**, *116*, 9399–9400. [[CrossRef](#)] [[PubMed](#)]
2. Bissel, R.A.; Cordova, E.; Kaifer, A.E.; Stoddart, J.F. A chemically and electrochemically switchable molecular shuttle. *Nature* **1994**, *369*, 133–137. [[CrossRef](#)]
3. Kolchinski, A.G.; Busch, D.H.; Alcock, N.W. Gaining control over molecular threading: Benefits of second coordination sites and aqueous-organic interfaces in rotaxane synthesis. *J. Chem. Soc. Chem. Commun.* **1995**, 1289–1291. [[CrossRef](#)]
4. Martinez-Diaz, M.-V.; Spencer, N.; Stoddart, J.F. The Self-Assembly of a Switchable [2]Rotaxane. *Angew. Chem. Int. Ed. Engl.* **1997**, *36*, 1904–1907. [[CrossRef](#)]
5. Gasa, T.; Spruell, J.M.; Dichtel, W.R.; Sorensen, T.J.; Philp, D.; Stoddart, J.F.; Kuzmic, P. Complexation between Methyl Viologen (Paraquat) Bis (Hexafluorophosphate) and Dibenzo[24]Crown-8 Revisited. *Chem. Eur. J.* **2009**, *15*, 106–116. [[CrossRef](#)] [[PubMed](#)]
6. Álvaro, M.; Ferrer, B.; Garcia, H.; Palomares, E.J.; Balzani, V.; Credi, A.; Venturi, M.; Stoddart, J.F.; Wenger, S. Photochemistry of a dumbbell-shaped multicomponent system hosted inside the mesopores of Al/MCM-41 aluminosilicate. Generation of long-lived viologen radicals. *J. Phys. Chem. B* **2003**, *107*, 14319–14325. [[CrossRef](#)]
7. Braunschweig, A.B.; Ronconi, C.M.; Han, J.Y.; Arico, F.; Cantrill, S.J.; Stoddart, J.F.; Khan, S.I.; White, A.J.P.; Williams, D.J. Pseudorotaxanes and rotaxanes formed by viologen derivatives. *Eur. J. Org. Chem.* **2006**, 1857–1866. [[CrossRef](#)]
8. Allwood, B.L.; Shahriari-Zavareh, H.; Stoddart, J.F.; Williams, D.J. Complexation of Paraquat and Diquat by a bismetaphenylene-32-crown-10 derivative. *J. Chem. Soc. Chem. Commun.* **1987**, 1058–1061. [[CrossRef](#)]
9. Allwood, B.L.; Spencer, N.; Shahriari-Zavareh, H.; Stoddart, J.F.; Williams, D.J. Complexation of Paraquat by a bisparaphenylene-34-crown-10 derivative. *J. Chem. Soc. Chem. Commun.* **1987**, 1064–1066. [[CrossRef](#)]
10. Huang, F.; Zakharov, L.N.; Rheingold, A.L.; Ashraf-Khorassani, M.; Gibson, H.W. Synthesis of a symmetric cylindrical bis (crown ether) host and its complexation with paraquat. *J. Org. Chem.* **2005**, *70*, 809–813. [[CrossRef](#)] [[PubMed](#)]

11. Loeb, S.J. Rotaxanes as ligands: From molecules to materials. *Chem. Soc. Rev.* **2007**, *36*, 226–235. [[CrossRef](#)] [[PubMed](#)]
12. Loeb, S.J.; Tiburcio, J.; Vella, S.J.; Wisner, J.A. A versatile template for the formation of [2]pseudorotaxanes. 1, 2-Bis (pyridinium) ethane axles and 24-crown-8 ether wheels. *Org. Biomol. Chem.* **2006**, *4*, 667–680. [[CrossRef](#)] [[PubMed](#)]
13. Loeb, S.J.; Wisner, J.A. [2]Rotaxane molecular shuttles employing 1,2-bis(pyridinium)ethane binding sites and dibenzo-24-crown-8 ethers. *Chem. Commun.* **2000**, 1939–1940. [[CrossRef](#)]
14. Hoffart, D.J.; Tiburcio, J.; De la Torre, A.; Knight, L.K.; Loeb, S. Cooperative Ion–Ion Interactions in the Formation of Interpenetrated Molecules. *Angew. Chem. Int. Ed.* **2008**, *47*, 97–101. [[CrossRef](#)] [[PubMed](#)]
15. Loeb, S.J.; Wisner, J.A. A New Motif for the Self-Assembly of [2]Pseudorotaxanes; 1, 2-Bis (pyridinium) ethane Axles and [24] Crown-8 Ether Wheels. *Angew. Chem. Int. Ed.* **1998**, *37*, 2838–2840. [[CrossRef](#)]
16. Loeb, S.J.; Tiburcio, J.; Vella, S.J. A mechanical “flip-switch”. Interconversion between co-conformations of a [2]rotaxane with a single recognition site. *Chem. Commun.* **2006**, 1598–1600. [[CrossRef](#)] [[PubMed](#)]
17. Mercer, D.J.; Vella, S.J.; Guertin, L.; Suhan, N.D.; Tiburcio, J.; Vukotic, V.N.; Wisner, J.A.; Loeb, S.J. Rotaxanes Based on the 1, 2-Bis (pyridinio) ethane–24-Crown-8 Templating Motif. *Eur. J. Org. Chem.* **2011**, *9*, 1763–1770. [[CrossRef](#)]
18. Tramontozzi, D.A.; Suhan, N.D.; Eichhorn, S.H.; Loeb, S.J. The effect of incorporating Fréchet dendrons into rotaxanes and molecular shuttles containing the 1,2-bis(pyridinium) ethane–[24]crown-8 templating motif. *Chem. Eur. J.* **2010**, *16*, 4466–4476. [[CrossRef](#)] [[PubMed](#)]
19. Bolla, M.A.; Tiburcio, J.; Loeb, S.J. Characterization of a slippage stopper for the 1,2-bis (pyridinium)ethane–[24]crown-8 ether [2]pseudorotaxane motif. *Tetrahedron* **2008**, *64*, 8423–8428. [[CrossRef](#)]
20. Hoffart, D.J.; Loeb, S.J. Metal–organic rotaxane frameworks: Three-dimensional polyrotaxanes from Lanthanide-ion nodes, pyridinium *N*-oxide axles, and crown-ether wheels. *Angew. Chem. Int. Ed. Engl.* **2005**, *44*, 901–904. [[CrossRef](#)] [[PubMed](#)]
21. Davidson, G.J.E.; Loeb, S.J. Channels and cavities lined with interlocked components: Metal-based polyrotaxanes that utilize pyridinium axles and crown ether wheels as ligands. *Angew. Chem. Int. Ed. Engl.* **2003**, *42*, 74–77. [[CrossRef](#)] [[PubMed](#)]
22. Coutrot, F. A Focus on Triazolium as a Multipurpose Molecular Station for pH-Sensitive Interlocked Crown Ether-Based Molecular Machines. *ChemistryOpen* **2015**, *4*, 556–576. [[CrossRef](#)] [[PubMed](#)]
23. Waelès, P.; Riss-Yaw, B.; Coutrot, F. Synthesis of a pH-Sensitive Hetero[4]Rotaxane Molecular Machine that Combines [c2]Daisy and [2]Rotaxane Arrangements. *Chem. Eur. J.* **2016**, *22*, 6837–6845. [[CrossRef](#)] [[PubMed](#)]
24. Legigan, T.; Riss-Yaw, B.; Clavel, C.; Coutrot, F. Active Esters as Pseudo-Stopppers for Slippage Synthesis of [2]Pseudorotaxane Building-Blocks: A Straightforward Route to Multi-Interlocked Molecular Machines. *Chem. Eur. J.* **2016**, *22*, 8835–8847. [[CrossRef](#)] [[PubMed](#)]
25. Waelès, P.; Fournel-Marotte, K.; Coutrot, F. Distinguishing two Ammonium and a Triazolium Sites of Interactions in a Three-Station [2]Rotaxane Molecular Shuttle. *Chem. Eur. J.* **2017**, *23*, 11529–11539. [[CrossRef](#)] [[PubMed](#)]
26. Waelès, P.; Clavel, C.; Fournel-Marotte, K.; Coutrot, F. Synthesis of Triazolium-Based Mono- and Tris-branched [1]Rotaxanes Using a Molecular Transporter of Dibenzo-24-Crown-8. *Chem. Sci.* **2015**, *6*, 4828–4836. [[CrossRef](#)] [[PubMed](#)]
27. Meng, Z.; Han, Y.; Wang, L.-N.; Xiang, J.-F.; He, S.-G.; Chen, C.F. Stepwise Motion in a Multivalent [2](3) catenane. *J. Am. Chem. Soc.* **2015**, *137*, 9739–9745. [[CrossRef](#)] [[PubMed](#)]
28. Yao, J.; Fu, X.; Zheng, X.-L.; Cao, Z.Q.; Qu, D.-H. Two functional [2]rotaxanes featuring efficient intercomponent interactions between chromophores. *Dyes Pigments* **2015**, *121*, 13–20. [[CrossRef](#)]
29. Alvarez, C.M.; Barbero, H.; Miguel, D. Multivalent Molecular Shuttles—Effect of Increasing the Number of Centers in Switchable Catalysts. *Eur. J. Org. Chem.* **2015**, *2015*, 6631–6640. [[CrossRef](#)]
30. Ragazzon, G.; Credi, A.; Colasson, B. Thermodynamic Insights on a Bistable Acid–Base Switchable Molecular Shuttle with Strongly Shifted Co-conformational Equilibria. *Chem. Eur. J.* **2017**, *23*, 2149–2156. [[CrossRef](#)] [[PubMed](#)]
31. Huang, F.; Slebodnick, C.; Ratliff, A.E.; Gibson, H.W. Bis (m-phenylene)-32-crown-10/monopyridinium [2]pseudorotaxanes. *Tetrahedron Lett.* **2005**, *46*, 6019–6022. [[CrossRef](#)]

32. Cheng, P.-N.; Lin, C.-F.; Liu, Y.H.; Lai, C.-C.; Peng, S.M.; Chiu, S.-H. [3]Pseudorotaxane-like complexes formed between bipyridinium dications and bis-p-xylyl [26]crown-6. *Org. Lett.* **2006**, *8*, 435–438. [[CrossRef](#)] [[PubMed](#)]
33. Huang, Y.-L.; Lin, C.-F.; Cheng, P.-N.; Lai, C.-C.; Liu, Y.-H.; Peng, S.-M.; Chiu, S.-H. Bis-p-xylyl [26]crown-6/pyridinium ion recognition: One-pot synthesis of molecular shuttles. *Tetrahedron Lett.* **2008**, *49*, 1665–1669. [[CrossRef](#)]
34. Coutrot, F.; Busseron, E. Controlling the Chair Conformation of a Mannopyranose in a Large-Amplitude [2]Rotaxane Molecular Machine. *Chem. Eur. J.* **2009**, *15*, 5186–5190.
35. Riss-Yaw, B.; Waeles, P.; Coutrot, F. Reverse Anomeric Effect in Large-Amplitude Pyridinium Amide-Containing Mannosyl [2]Rotaxane Molecular Shuttles. *ChemPhysChem* **2016**, *17*, 1860–1869. [[CrossRef](#)] [[PubMed](#)]
36. Busseron, E.; Romuald, C.; Coutrot, F. Very Contracted to Extended co-Conformations with or without Oscillations in Two- and Three-Station [c2]Daisy Chains. *J. Org. Chem.* **2010**, *75*, 6516–6531.
37. Busseron, E.; Romuald, C.; Coutrot, F. Bistable or Oscillating State Depending on Station and Temperature in Three-Station Glycorotaxane Molecular Machines. *Chem. Eur. J.* **2010**, *16*, 10062–10073. [[CrossRef](#)] [[PubMed](#)]
38. Zhu, K.; Vukotic, V.N.; Loeb, S.J. Acid-Base Switchable [2]- and [3]Rotaxane Molecular Shuttles with Benzimidazolium and Bis(pyridinium) Recognition Sites. *Chem. Asian J.* **2016**, *11*, 3258–3266. [[CrossRef](#)] [[PubMed](#)]
39. Li, L.; Clarkson, G.J. New Bis(benzimidazole) Cations for Threading through Dibenzo-24-crown-8. *Org. Lett.* **2007**, *9*, 497–500. [[CrossRef](#)] [[PubMed](#)]
40. Castillo, D.; Astudillo, P.; Mares, J.; González, F.J.; Vela, A.; Tiburcio, J. Chemically controlled self-assembly of [2]pseudorotaxanes based on 1,2-bis(benzimidazolium)ethane cations and 24-crown-8 macrocycles. *Org. Biomol. Chem.* **2007**, *5*, 2252–2256. [[CrossRef](#)] [[PubMed](#)]
41. Noujeim, N.; Zhu, K.; Vukotic, V.N.; Loeb, S.J. [2]Pseudorotaxanes from T-shaped benzimidazolium axles and [24]Crown-8 wheels. *Org. Lett.* **2012**, *14*, 2484–2487. [[CrossRef](#)] [[PubMed](#)]
42. Kihara, N.; Hashimoto, M.; Takata, T. Behavior of Ferrocene-Containing Rotaxane: Transposition of the Rotaxane Wheel by Redox Reaction of a Ferrocene Moiety Tethered at the End of the Axle. *Org. Lett.* **2004**, *6*, 1693–1696. [[CrossRef](#)] [[PubMed](#)]
43. Hsueh, S.-Y.; Kuo, C.-T.; Lu, T.-W.; Lai, C.-C.; Liu, Y.-H.; Hsu, H.-F.; Peng, S.-M.; Chen, C.-H.; Chiu, S.-H. Acid/Base- and Anion-Controllable Organogels Formed From a Urea-Based Molecular Switch. *Angew. Chem. Int. Ed.* **2010**, *49*, 9170–9173. [[CrossRef](#)] [[PubMed](#)]
44. Kwan, C.-S.; Chan, A.S.C.; Leung, K.C.-F. A Fluorescent and Switchable Rotaxane Dual Organocatalyst. *Org. Lett.* **2016**, *18*, 976–979. [[CrossRef](#)] [[PubMed](#)]
45. Valentina, S.; Ogawa, T.; Nakazono, K.; Aoki, D.; Takata, T. Efficient Synthesis of Cyclic Block Copolymers by Rotaxane Protocol by Linear/Cyclic Topology Transformation. *Chem. Eur. J.* **2016**, *22*, 8759–8762. [[CrossRef](#)] [[PubMed](#)]
46. Aoki, D.; Takata, T. Mechanically linked supramolecular polymer architectures derived from macromolecular [2]rotaxanes: Synthesis and topology transformation. *Polymer* **2017**, *128*, 276–296. [[CrossRef](#)]
47. Sawada, J.; Aoki, D.; Takata, T. Vinylic rotaxane cross-linker comprising different axle length for the characterization of rotaxane cross-linked polymers. *Macromol. Symp.* **2017**, *372*, 115–119. [[CrossRef](#)]
48. Ogawa, T.; Nakazono, K.; Aoki, D.; Uchida, S.; Takata, T. Effective approach to cyclic polymer from linear polymer: Synthesis and transformation of macromolecular [1]rotaxane. *ACS Macro Lett.* **2015**, *4*, 343–347. [[CrossRef](#)]
49. Aoki, D.; Aibara, G.; Uchida, S.; Takata, T. A rational entry to cyclic polymers via selective cyclization by self-assembly and topology transformation of linear polymers. *J. Am. Chem. Soc.* **2017**, *139*, 6791–6794. [[CrossRef](#)] [[PubMed](#)]
50. Sato, H.; Aoki, D.; Takata, T. Synthesis and Star/Linear Topology Transformation of a Mechanically Linked ABC Terpolymer. *ACS Macro Lett.* **2016**, *5*, 699–703. [[CrossRef](#)]
51. Matsumura, T.; Ishiwari, F.; Koyama, Y.; Takata, T.C.-C. Bond-Forming Click Synthesis of Rotaxanes Exploiting Nitrile N-Oxide. *Org. Lett.* **2010**, *12*, 3828–3831. [[CrossRef](#)] [[PubMed](#)]
52. Tachibana, Y.; Kawasaki, H.; Kihara, N.; Takata, T. Sequential O- and N-acylation protocol for high-yield preparation and modification of rotaxanes: Synthesis, functionalization, structure, and intercomponent interaction of rotaxanes. *J. Org. Chem.* **2006**, *71*, 5093–5104. [[CrossRef](#)] [[PubMed](#)]

53. Smukste, I.; House, B.E.; Smithrud, D.B. Host-[2]rotaxane: Advantage of converging functional groups for guest recognition. *J. Org. Chem.* **2003**, *68*, 2559–2571. [[CrossRef](#)] [[PubMed](#)]
54. Dvornikovs, V.; House, B.E.; Kaetzel, M.; Dedman, J.R.; Smithrud, D.B. Host-[2]rotaxanes as cellular transport agents. *J. Am. Chem. Soc.* **2003**, *125*, 8290–8301. [[CrossRef](#)] [[PubMed](#)]
55. Zehnder, D.W.; Smithrud, D.B. Facile synthesis of rotaxanes through condensation reactions of DCC-[2]rotaxanes. *Org. Lett.* **2001**, *3*, 2485–2487. [[CrossRef](#)] [[PubMed](#)]
56. Bao, X.; Isaacs, I.; Drew, A.F.; Smithrud, D.B. Determining the intracellular transport mechanism of a cleft-[2]rotaxane. *J. Am. Chem. Soc.* **2006**, *128*, 12229–12238. [[CrossRef](#)] [[PubMed](#)]
57. Smukste, I.; Smithrud, D.B. Structure-function relationship of amino acid-[2]rotaxanes. *J. Org. Chem.* **2003**, *68*, 2547–2558. [[CrossRef](#)] [[PubMed](#)]
58. Romuald, C.; Cazal, G.; Enjalbal, C.; Coutrot, F. Straightforward Synthesis of a Double-Lasso Macrocyclic from a Nonsymmetrical [c2]Daisy Chain. *Org. Lett.* **2013**, *15*, 184–187. [[CrossRef](#)] [[PubMed](#)]
59. Schwesinger, R.; Willaredt, J.; Schlemper, H.; Keller, M.; Schmitt, D.; Fritz, H. Novel, Very Strong, Uncharged Auxiliary Bases; Design and Synthesis of Monomeric and Polymer-Bound Triaminoiminophosphorane Bases of Broadly Varied Steric Demand. *Chem. Ber.* **1994**, *127*, 2435–2454. [[CrossRef](#)]
60. Nakazono, K.; Takata, T. Neutralization of a sec-Ammonium Group Unusually Stabilized by the “Rotaxane Effect”: Synthesis, Structure, and Dynamic Nature of a “Free” sec-Amine/Crown Ether-Type Rotaxane. *Chem. Eur. J.* **2010**, *16*, 13783–13794. [[CrossRef](#)] [[PubMed](#)]
61. Riss-Yaw, B.; Clavel, C.; Laurent, P.; Coutrot, F. The relationship between the conformational degree of freedom of template-containing threads and slippage in the formation of [2]rotaxane building blocks. *Chem. Commun.* **2017**, *53*, 10874–10877. [[CrossRef](#)] [[PubMed](#)]



© 2017 by the authors. Licensee MDPI, Basel, Switzerland. This article is an open access article distributed under the terms and conditions of the Creative Commons Attribution (CC BY) license (<http://creativecommons.org/licenses/by/4.0/>).